# Uncertainty Quantification of Soil–Structure Interface Properties with an Enhanced Hypoplastic Interface Model

Hai-Lin Wang[1]; Yin-Fu Jin[2]; Zhen-Yu Yin[3]; and Xiao-Qiang Gu[4]

**Abstract:** Numerous studies have been carried out to characterize uncertainties of soil properties, and lots of multivariate databases have been compiled to make the characterization of uncertainties more realistic. However, when it comes to complex situations, that is, for complex critical state constitutive models and soil–structure interface properties, the uncertainty quantification becomes a challenge. This paper aims to quantify the uncertainties of the soil–structure interface properties from laboratory tests. A framework of uncertainty quantification based on a simplified two-dimensional Monte Carlo simulation is first proposed. To validate the performance of the framework, an enhanced hypoplastic interface model considering particle breakage is then proposed and employed in the uncertainty quantification framework. The CMA-ES algorithm is then used to calibrate the uncertainties based on the framework and the hypoplastic soil–structure interface model. The results showed the proposed framework with the enhanced model can capture the uncertainties of the soil–structure interface properties. In the studied experiments, 30 out of 42 experimental curves were found to be well calibrated based on the Kolmogorov–Smirnov normality test. Furthermore, to obtain acceptable results, based on the calibration-validation process, the effect of the selection of experiments on the calibration performance is discussed. Some suggestions on how to choose experiments to calibrate the soil–structure interface properties are summarized, which should be helpful in practice. **DOI: 10.1061/IJGNAI.GMENG-9248**. 

**Author keywords:** Soil–structure interface; Constitutive model; Parameter identification; Elastoplasticity; Optimization; Sensitivity analysis.



## Introduction

In geotechnical engineering, an important task is to obtain design parameters according to the site survey report. Extensive statistical data showed that there is a wide range of uncertainty in geotechnical parameters. The necessity of considering the uncertainty of geotechnical parameters has been proved in many studies (Phoon and Kulhawy 1999; Papaioannou and Straub 2017). Different types of uncertainties are involved in geotechnical engineering, such as uncertainties of soil properties, constitutive models, boundary conditions, loading conditions, and uncertainties caused by measurement error (Mašín 2015). The study of uncertainties in soil properties has become the focus of researchers in the last twenty years since it plays a significant role in the reliability-based design in geotechnical engineering. In this area, studies focus on the uncertainty characterization of soil properties extracted in different conditions combined with random field simulations, such as uncertainty characterization of soil properties in an homogeneous soil layer (Tang 1984), slope stability (Zhang et al. 2003), and pullout resistance of soil nails (Zhang et al. 2009). In terms of reliability-based design, or random field simulation, the difficulties have nothing to do with the theory, but have everything to do with the statistical characterization of the soil properties (Phoon 2020). To make the characterization of the soil properties more realistic, researchers have compiled tons of multivariate databases of soil properties over the past decade (Ching and Phoon 2014; D'Ignazio et al. 2016), over clay, sand, and rock in a wide range of regions.

The compilation of such general soil properties databases can be very useful to geotechnical engineering, making it possible to conduct reliability-based geotechnical design. However, when it comes to complicated situations, such databases are usually not available. For example, in conditions where complex critical state constitutive models are used, the soil properties usually lack deep investigations, the uncertainties of the soil properties are not well recognized, and in other conditions such as the soil–structure interfaces, the uncertainties of the soil–structure properties are not well studied in the past, so it might be difficult to characterize the uncertainties of the soil–structure properties. In these conditions, putting aside the uncertainties of the soil properties, general geotechnical design is still possible by using the model calibration method to obtain acceptable model parameters from the experiments. In the framework of the model calibration, estimation of the uncertainties of the soil properties is actually possible (Jung et al. 2016), although it has been rarely studied in the past in the domain of geotechnical engineering, especially in the domain of soil–structure interfaces.

The soil–structure interaction is critically important for the geotechnical engineering structures, especially for soil anchors (Seo and Pelecanos 2018; Singh and SivakumarBabu 2010), suction caissons (Skau et al. 2019), pile foundations (Carbonari et al. 2018), tunnels (Sayed et al. 2019), and retaining walls (Psarropoulos et al. 2022). The soil–structure interface, known as the shearing zone between the soil and the structure, has attracted the research

[1]Ph.D. Candidate, Dept. of Civil and Environmental Engineering, The Hong Kong Polytechnic Univ., Hong Kong 999077, China; Dept. of Geotechnical Engineering, College of Civil Engineering, Tongji Univ., Shanghai 200092, China. Email: hailin.wang@connect.polyu.hk

[2]Professor, College of Civil and Transportation Engineering, Shenzhen Univ., Shenzhen 518060, China. Email: yinfujin@szu.edu.cn

[3]Professor, Dept. of Civil and Environmental Engineering, The Hong Kong Polytechnic Univ., Hong Kong 999077, China (corresponding author). Email: zhenyu.yin@polyu.edu.hk

[4]Professor, Dept. of Geotechnical Engineering, College of Civil Engineering, Tongji Univ., Shanghai 200092, China. Email: guxiaoqiang@tongji.edu.cn

Note. This manuscript was submitted on May 25, 2023; approved on December 26, 2023; published online on April 3, 2024. Discussion period open until September 3, 2024; separate discussions must be submitted for individual papers. This paper is part of the ***International Journal of Geomechanics***, © ASCE, ISSN 1532-3641.

interest of many scholars. To characterize the mechanical behavior of the interface, direct shear tests (Frost et al. 2002; DeJong and Westgate 2009), simple shear tests (Uesugi and Kishida 1986; Fakharian and Evgin 2000), ring torsion shear tests (Desai et al. 2005; Yasufuku and Ochiai 2005), and annular shear tests (Brumund and Leonards 1973; Koval et al. 2011) are conducted to investigate the behaviors of the soil–structure interface. To simulate these soil–structure interface behaviors, numerous models have been proposed, such as the exponential model (Yang and Yin 2021a), the hypoplastic model (Arnold and Herle 2006; Stutz et al. 2016; Stutz and Masin 2017), and the elastoplastic models (Desai and Ma 1992; Mortara 2001; Hu and Pu 2003, 2004; Lashkari 2013).

Although there has been a lot of research on the soil–structure interface in the past, the investigation of the uncertainties of the soil–structure properties is still a new topic. This paper aims to introduce the uncertainty quantification of the soil–structure properties based on an enhanced hypoplastic soil–structure interface model. The paper is organized as follows: first, the framework of the uncertainty quantification of the soil–structure properties is proposed; second, the enhanced hypoplastic soil–structure interface model is introduced; third, the introduced hypoplastic model combined with the uncertainty quantification framework is evaluated; finally, to obtain acceptable soil–structure properties from the experiments, some suggestions on the selection of experiments to be conducted to do the calibration are given.

## Methodology

In this section, the framework of the uncertainty quantification based on the optimization method is first introduced. An enhanced hypoplastic soil–structure interface model is then proposed to be used in the uncertainty quantification framework. Lastly, the procedures of the uncertainty quantification are summarized.

### *Framework of Uncertainty Quantification*

In this section, it is assumed that the uncertainty of the soil property is the only uncertainty source, that is, the model uncertainty, sampling uncertainty, and other uncertainties are all neglected. The uncertainties of the soil properties are generally estimated based on compiled multivariate databases of soil properties (i.e., Ching and Phoon 2014; D'Ignazio et al. 2016). However, in complex situations where such databases are not available, they may be estimated from the inverse analysis of experiments under the assumption that the variability of the experiments is only caused by the variability of the soil properties. Such estimations can be found in the literature (Jung et al. 2016; Youn et al. 2011; Zhan et al. 2011; Fender et al. 2014; Warner et al. 2015; Kennedy and O'Hagan 2001; Higdon et al. 2008; Liu et al. 2008; Park et al. 2016). Since the constitutive model is usually too complicated to obtain an inverse model, numerical methods must be used to solve the inverse problem. In general, there are two groups of methods to solve the inverse problem, optimization-based model calibration (Jung et al. 2016) and Bayesian-based model calibration (Park et al. 2016). The optimization-based model calibration provides a straightforward method to solve the inverse problem by minimizing an objective function that describes the difference between the experiments and simulations. The Bayesian-based model calibration takes the prior knowledge of the material properties into consideration, and the posterior distribution is obtained by Bayes' theorem. Due to the fact that the Bayesian-based model calibration requires prior knowledge of the material properties and a statistical description of the measured experimental data (i.e., to calculate the likelihood function) that is usually difficult to obtain for an advanced constitutive model, the optimization-based model calibration is used in this paper.

#### Calibration Metrics

The objective function is the key to successful calibrations in optimization-based model calibration. The objective function describes the difference between the experiments and simulations. To consider uncertainty in the objective function, the system inputs ($\mathbf{X}$) and system responses ($\mathbf{Y}$) are considered random variables. The predicted and measured system responses $\mathbf{Y}_{\text{pre}}$ and $\mathbf{Y}_{\text{obs}}$ can be uncertain due to various sources, including model bias, measurement errors, disturbance of applied loading, or boundary conditions. Assuming the parameter uncertainty is the only source of uncertainty, showing that the observations can be considered as the true system responses and the predicted system responses are uncertain only because of parameter uncertainty, then we have

$$\mathbf{Y}_{\text{obs}} = \mathbf{Y}_{\text{pre}}(\mathbf{X}) + e \approx \mathbf{Y}_{\text{pre}}(\mathbf{X}) \tag{1}$$

where $e$ represents all kinds of other uncertainties that can be ignored. Model calibration is the process to solve the preceding equation. Since the constitutive model is usually too complicated to obtain an analytical solution to the preceding equation, an optimization method is required to solve the equation:

$$\mathbf{X} = \mathbf{Y}_{\text{pre}}^{-1}(\mathbf{Y}_{\text{obs}}) \Longrightarrow \mathbf{X} \approx \arg\min_{\mathbf{X}} \left\{ \text{dist}\left[\mathbf{Y}_{\text{obs}}, \mathbf{Y}_{\text{pre}}\right] \right\} \tag{2}$$

where dist$(\cdot)$ is a function that describes the distance between the predictions and observations.

If no uncertainty is considered, representing $\mathbf{X}$ is considered as a deterministic variable, and the dist function can be expressed as the root mean square error (RMSE) of the relative difference between the predictions and observations:

$$\text{dist}\left[\mathbf{Y}_{\text{obs}}, \mathbf{Y}_{\text{pre}}(\mathbf{X})\right] = \sum_{i=1}^{m} l_i \sqrt{\frac{1}{n}\sum_{j=1}^{n}\left[\frac{\mathbf{Y}_{\text{pre},ij}(\mathbf{X}) - \mathbf{Y}_{\text{obs},ij}}{\text{T}\left(\mathbf{Y}_{\text{obs},i}\right)}\right]^2} \tag{3}$$

where $\mathbf{X}$ represents the calibrated model parameters, $\text{T}(\mathbf{Y}_{\text{obs},i})$ represents the range of the observations (i.e., $\text{T}(\mathbf{Y}_{\text{obs},i}) = \max_{j\in[1,\,n]}(\mathbf{Y}_{\text{obs},ij}) - \min_{j\in[1,\,n]}(\mathbf{Y}_{\text{obs},ij})$), the index $i$ indicates different types of experimental tests (i.e., CNL, CNS, CV tests) or different types of tests variables (i.e., shear stress, normal displacement, etc.), the index $j$ indicates measured points of a certain variable in a certain test, and $m$ and $n$ are the number of tests/variables and measured points, respectively. The weights $l_i$ represent the importance of different tests and variables, and $l_i = 1/m$ is chosen for simplicity.

To consider parameter uncertainty, the objective function must be reformulated. Since $\mathbf{X}$ is a multivariate random variable, the predicted system response $\mathbf{Y}_{\text{pre}}(\mathbf{X})$ is also a random variable. Given normally distributed random variables $\mathbf{X}$, assume the predicted system response $\mathbf{Y}_{\text{pre}}(\mathbf{X})$ is still normally distributed. The mean and variance of the predicted system response $\mathbf{Y}_{\text{pre}}(\mathbf{X})$ can be obtained based on the Monte Carlo simulation (MCS; detailed calculation can be found in the following section):

$$\mathbf{Y}_{\text{pre}}(\mathbf{X}) \sim \mathcal{N}(\boldsymbol{\mu}, \boldsymbol{\Sigma}) \tag{4}$$

Then, it is possible to calculate the distance between the predicted system response $\mathbf{Y}_{\text{pre}}(\mathbf{X})$ and the measured system response $\mathbf{Y}_{\text{obs}}$ based on the uncertainty quantification metrics, such as the likelihood function, the average calibration metrics based on the quantiles or centered prediction intervals (Chung et al. 2021), the group calibration rules (Kleinberg et al. 2016), and the proper

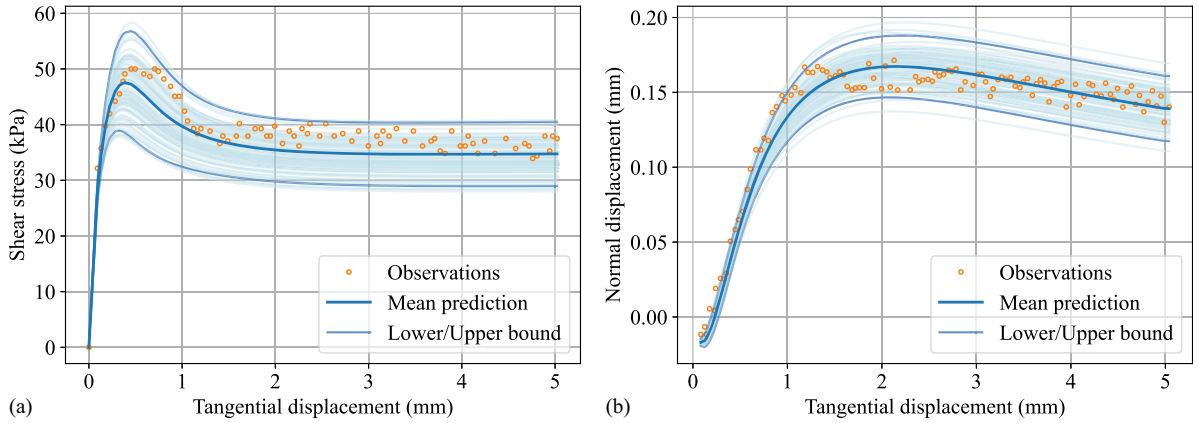


**Fig. 1.** Illustration of the predicted system response considering parameter uncertainty: (a) shear stress; and (b) normal displacement.

scoring rules (Gneiting et al. 2007):

$$\text{dist}\left[\mathbf{Y}_{\text{obs}}, \mathbf{Y}_{\text{pre}}(\mathbf{X})\right] = \mathbf{D}\left(\mathbf{Y}_{\text{obs}}, \mathbf{Y}_{\text{pre}}(\boldsymbol{\mu}, \boldsymbol{\Sigma})\right) \tag{5}$$

where $\mathbf{D}$ can have multiple forms to evaluate the calibration performance of the proposed model, such as the RMSE, mean absolute error (MAE), miscalibration area (MA), negative log-likelihood (NLL), continuous ranked probability score (CRPS), negatively oriented check score, and the negatively oriented interval score (Chung et al. 2021), which are based on the predicted and observed quantiles. Compared with metrics such as the Kullback–Leibler divergence (Kullback and Leibler 1951), the advantage of the quantiles-based metrics is that they are bounded to 0 and 0.5 which is really convenient to use in the calibration. Furthermore, since the quantile function is the inverse of the cumulative distribution function (CDF), the predicted and observed quantile figure can be useful to do the Kolmogorov–Smirnov (KS) normality test. In this paper, the most commonly used RMSE is used to evaluate the calibration performance of the proposed model. The detailed calculation can be found in the following section.

The quantification of the predicted system response uncertainty [Eq. (4)] can be achieved by the MCS. To this end, the parameters are sampled according to their probability distributions, and the corresponding model runs are performed. However, the exact types and distribution parameters are not well-known since the goal of optimization-based model calibration is to get the optimized distribution parameters. Therefore, a two-dimensional MCS is required:

1. **Outer MCS**: the distribution parameters (i.e., mean and covariance matrix for normally distributed variables) of the model parameters are sampled by the optimizer;
2. **Inner MCS**: the model parameters are sampled according to their distribution parameters and the corresponding model runs are performed.

On the one hand, conducting the two-dimensional MCS is extremely time-consuming, such that even simulations with 100 samples for each MCS would require 10,000 model runs. On the other hand, the optimization algorithm requires the objective function to be deterministic so that the optimizer can obtain a clear optimization direction, which requires a large number of model runs for the inner MCS. Therefore, an approximate uncertainty analysis method (Hofer et al. 2002) is used in this study. In this method, the random field structure (defined by the normalized random variables) of the inner MCS is fixed during the optimization process, resulting in a deterministic objective function that can be used in the optimization. Assuming the model parameters are normally distributed (the assumption of the normal distribution is not necessary for the framework, but a change to other distributions is quite straightforward; we just need to update the sampling step), $\mathbf{Z}$ is a multivariate random variable with zero mean and unit variance, and $\boldsymbol{\mu}$ and $\boldsymbol{\Sigma}$ are the mean and covariance matrix of the samples, then the predicted system response $\mathbf{Y}_{\text{pre}}(\mathbf{X})$ can be obtained by

$$\mathbf{Y}_{\text{pre}}(\mathbf{X}) = \mathbf{Y}_{\text{pre}}(\boldsymbol{\mu} + \mathbf{AZ}), \quad \text{where } \boldsymbol{\Sigma} = \mathbf{AA}^T \tag{6}$$

In the inner MCS, the samples of $\mathbf{Z}$ are generated before the optimization process and fixed during the optimization process so that $\mathbf{Y}_{\text{pre}}(\mathbf{X})$ is a deterministic function of $\boldsymbol{\mu}$ and $\boldsymbol{\Sigma}$.

Fig. 1 illustrates an example of the predicted system response of the soil–structure interface experiments considering the parameter uncertainty which is obtained by the MCS. The lower and upper bounds are the 95% confidence intervals of the predictions. The predicted system responses based on 100 samples of model parameters generated by the statistical distribution of the model parameters shown in Eq. (6) are all plotted with thinner lines in Fig. 1. With the assumption that the predictions are normally distributed (the real distribution type is impossible to be determined because of the complex constitutive model and this assumption will be validated in the results section), the means and standard deviations of the predictions at every point can be estimated by the predictions of the samples:

$$\mathbf{Y}_{\text{pre}}(\gamma) \sim \mathcal{N}[\boldsymbol{\mu}(\gamma), \boldsymbol{\sigma}(\gamma)] \tag{7}$$

where $\gamma$ is the tangential displacement and it can be any other variables, and $\boldsymbol{\mu}(\gamma)$ and $\boldsymbol{\sigma}(\gamma)$ are the estimated mean and standard deviation of the predictions at point $\gamma$, respectively. The predictions can then be normalized to the standard normal distribution at every point:

$$\bar{\mathbf{Y}}_{\text{pre}}(\gamma) = \frac{\mathbf{Y}_{\text{pre}}(\gamma) - \boldsymbol{\mu}(\gamma)}{\boldsymbol{\sigma}(\gamma)} \sim \mathcal{N}(0, 1) \tag{8}$$

The predicted and observed quantiles at specific proportions can be obtained:

$$\bar{\mathbf{Y}}_{\text{pre}}^{-1}(p) = Q(p) \quad \text{and} \quad \bar{\mathbf{Y}}_{\text{obs}}^{-1}(p) = \hat{F}^{-1}(p) \tag{9}$$

where $Q(p)$ is the quantile function [also called the percent point function ppf($p$) or inverse CDF $F^{-1}(p)$] of the standard normal distribution and $\hat{F}^{-1}(p)$ is the inverse empirical CDF of the observations.

Fig. 2 shows the observed quantiles versus the predicted quantiles for the preceding example. The fitness between the predicted and observed quantiles can then be evaluated by comparing the predicted and observed quantiles. Different metrics such as the RMSE can be used to quantify the fitness:

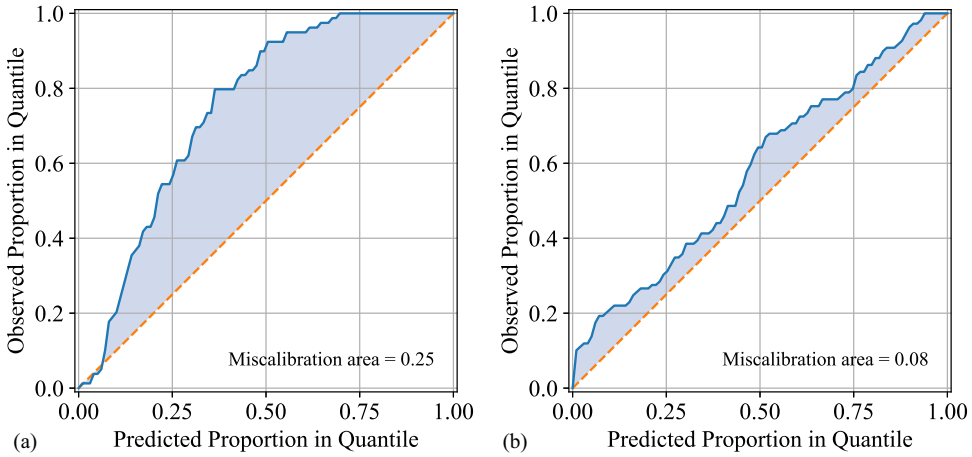


**Fig. 2.** Observed quantiles versus predicted quantiles: (a) shear stress; and (b) normal displacement.

$$\mathrm{dist}\left[\mathbf{Y}_{\mathrm{obs}}, \mathbf{Y}_{\mathrm{pre}}(\mathbf{X})\right] = \sum_{i=1}^{m} l_i \sqrt{\frac{1}{N}\sum_{j=1}^{n}\left[\bar{Y}_{\mathrm{pre}}^{-1}(p_j) - \bar{Y}_{\mathrm{obs}}^{-1}(p_j)\right]^2} \quad (10)$$

In Fig. 2, the corresponding predicted quantile is smaller than the observed quantile (the curve is above the line of $y = x$), showing the uncertainty of the parameters is overestimated, which is consistent with Fig. 1.

## Enhanced Hypoplastic Interface Model for the Uncertainty Quantification

In this section, an enhanced hypoplastic soil–structure interface model will be introduced to incorporate the uncertainty quantification framework.

### Basic Hypoplastic Model

The hypoplastic model adopts nonlinear equations to characterize the stress–strain relation. It was initially proposed by Kolymbas (1991). Wang et al. (2018) simplified the equation by combining the two nonlinear items and then applied the model to granular material considering the time-dependent behavior. The basic equation of the hypoplastic model consists of four parts (Wang et al. 2018):

$$\mathring{\boldsymbol{\sigma}} = I_{se}\left[c_1 \mathrm{tr}(\boldsymbol{\sigma})\dot{\boldsymbol{\varepsilon}} + c_2 \mathrm{tr}(\dot{\boldsymbol{\varepsilon}})\boldsymbol{\sigma} + c_3 \frac{\mathrm{tr}(\boldsymbol{\sigma}\dot{\boldsymbol{\varepsilon}})}{\mathrm{tr}(\boldsymbol{\sigma})}\boldsymbol{\sigma} + c_4(\boldsymbol{\sigma} + \boldsymbol{\sigma}^*)\|\dot{\boldsymbol{\varepsilon}}\| I_e\right] \quad (11)$$

where $\mathring{\boldsymbol{\sigma}}$ is Jaumann–Zaremba rate of the Cauchy stress, $c_i$ ($i = 1, 2, 3, 4$) are dimensionless material constants which can be determined using standardized laboratory tests (Wu and Bauer 1994), $\boldsymbol{\sigma}^* = \boldsymbol{\sigma} - 1/3 \cdot \mathrm{tr}(\boldsymbol{\sigma})\mathrm{I}$ is the deviatoric stress tensor, the $\mathrm{tr}(\cdot)$ operator is the trace of the matrix which is the summation of the elements on the main diagonal a matrix, and the $\|\cdot\|$ is the norm operator of the matrix. Here, $I_e$ is the critical state function to consider the critical state concept and $I_{se}$ is the stiffness function to overcome the shortcoming that the stress–strain curve is too stiff upon monotonic tests, expressed by (Wang et al. 2018)

$$I_e = \left(\frac{e}{e_c}\right)^{\alpha}, \quad I_{se} = \frac{\exp\left[\beta(e_c - e)\right]}{1 + r^2} \quad (12)$$

where $e$ and $e_c$ are the void ratio and critical void ratio, respectively, $\alpha$ and $\beta$ are two constants, and $r$ denotes the stress ratio $\|\boldsymbol{\sigma}^*\| - \mathrm{tr}(\boldsymbol{\sigma})$. The equation can be reduced for the interface condition:

$$\dot{\boldsymbol{\sigma}} = I_{se}\left[c_1 \sigma_n \dot{\boldsymbol{\varepsilon}} + c_2 \dot{\varepsilon}_n \boldsymbol{\sigma} + c_3 \frac{\sum(\boldsymbol{\sigma}\dot{\boldsymbol{\varepsilon}})}{\sigma_n}\boldsymbol{\sigma} + c_4(\boldsymbol{\sigma} + \boldsymbol{s})\|\dot{\boldsymbol{\varepsilon}}\| I_e\right] \quad (13)$$

where $\boldsymbol{\sigma} = [\sigma_n, \tau_s, \tau_t]^{\mathrm{T}}$, $\boldsymbol{s} = [0, \tau_s, \tau_t]^{\mathrm{T}}$, and $\boldsymbol{\varepsilon} = [\varepsilon_n, \gamma_s, \gamma_t]^{\mathrm{T}}$ are the stress vector, shear stress vector, and strain vector, respectively.

### Enhancements

Considering the simplicity, the following critical state function and stiffness function are used in this research:

$$I_e = \left(\frac{e}{e_c}\right)^{n_d}, \quad I_{se} = \left(\frac{e_c}{e}\right)^{n_p} \quad (14)$$

The equation of the critical void ratio $e_c$ can be found in much of the literature. The most common one is the linear equation in the

**Table 1.** Parameters of the hypoplastic interface model

| Category | Symbol | Note |
|---|---|---|
| Basic parameters | $R_d$ | The ratio of thickness to the median grain size |
| | $G_0$ | Reference shear modulus |
| | $n_g$ | An exponent in the equation of nonlinear shear modulus, usually 0.6 |
| | $\nu_i$ | Initial slope of $\varepsilon_n$–$\gamma$ curve |
| CSL parameters | $\phi_c$ | Critical friction angle |
| | $e_{\mathrm{ref}0}$ | Initial reference critical void ratio |
| | $\lambda$, $\xi$ | Constants that control the shape of the critical state line |
| | $n_p$, $n_d$ | Constants that control the effect of the density of the soil on the hardening/softening behaviors of the interface |
| Breakage parameters | $e_{\mathrm{refu}}$ | Ultimate reference critical void ratio due to particle breakage |
| | $\rho$ | A constant that controls the decreasing rate of the critical state line due to particle breakage |
| | $b$, $n_w$ | Constants that control the effect of the energy to the breakage index |

$e - \ln \sigma_n$ space ($e - \ln p'$ space in the material constitutive model) (Roscoe et al. 1958), and some other nonlinear equations have been proposed to improve the adaptability (Li and Wang 1998; Yin et al. 2018). This paper adopts the following equation proposed by Yin et al. (2018) considering its wide applicability:

$$e_c = e_{\text{ref}} \exp\left[-\lambda\left(\frac{\sigma_n}{p_{\text{at}}}\right)^{\xi}\right] \tag{15}$$

where $\lambda$ and $\xi$ are two constants controlling the shape of the critical state line (CSL), $p_{\text{at}}$ is the standard atmosphere pressure, and $e_{\text{ref}}$ is the reference critical void ratio corresponding to the critical void ratio when the normal stress is zero.

For the granular materials, due to particle breakage under a high-stress state, the critical void ratio tends to move downward in the $e - \ln \sigma_n$ space (Muir Wood and Maeda 2008; Yin et al. 2010). To consider the effect of particle breakage on the CSL, several equations have been proposed (Hu et al. 2011; Liu et al. 2014), with the following equation proposed by Liu et al. (2014):

$$e_{\text{ref}} = e_{\text{refu}} + (e_{\text{ref0}} - e_{\text{refu}}) \exp(-\rho B_r^*) \tag{16}$$

where $e_{\text{ref0}}$ and $e_{\text{refu}}$ are the initial and ultimate reference critical void ratio, respectively. Here, $\rho$ is a constant that controls the decreasing rate of the CSL, and $B_r^*$ is the breakage index. Research showed that the degree of particle breakage is related to the energy (Einav 2007), so a modified energy-based approach is suggested to calculate the breakage index (Jin et al. 2018a, 2018b; Wu et al. 2019; Yang and Yin 2021b):

$$B_r^* = \frac{w^{n_w}}{b + w^{n_w}}, \quad \text{with } w = \int \left(\langle \sigma_n \mathrm{d}\varepsilon_n \rangle + \tau \mathrm{d}\gamma\right) \tag{17}$$

where $\langle \cdot \rangle$ is the Macaulay brackets, and $b$, $\rho$, and $n_w$ are material constants.

To introduce the dependency of the stiffness on the density and the stress level, the expression of the nonlinear shear modulus $G$ (which will be used to determine the model coefficients $c_1$, $c_2$, $c_3$, $c_4$) suggested by Richart et al. (1970) has been adopted:

$$G = G_0 \frac{(2.97 - e)^2}{1 + e} \left(\frac{\sigma_n}{P_{\text{at}}}\right)^{n_g} \tag{18}$$

where $n_g$ is an exponent that usually takes the value of 0.6.

### Determination of Model Coefficients

Four model coefficients $c_i$ ($i = 1, 2, 3, 4$) can be calibrated with some simple soil–structure interface tests. In a constant volume interface test (similar to the undrained condition) with one-way shearing under monotonic loading, the normal displacement is fixed to zero, so considering the initial and final state, we have

$$\dot{\tau}_s|_{\dot{\gamma}_s=0} = c_1 \sigma_{n0} \dot{\gamma}_s I_{se0} = G\dot{\gamma}_s \tag{19}$$

$$\dot{\tau}_s|_{\dot{\gamma}_s\to\infty} = \sigma_n \dot{\gamma}_s \left(c_1 + c_3\mu^2 + 2c_4\mu\right) = 0 \tag{20}$$

where $\mu = \tan\phi_c = \tau_s/\sigma_n|_{\dot{\gamma}_s\to\infty}$. In a constant normal stress interface test with one-way shearing under monotonic loading, the normal stress is fixed, so considering the initial and final state, we have

$$\dot{\sigma}_n|_{\dot{\gamma}_s=0} = I_{se0}\sigma_n\dot{\varepsilon}_n\left[(c_1 + c_2 + c_3)\nu_i + c_4\sqrt{1 + \nu_i^2}I_{e0}\right] = 0 \tag{21}$$

$$\dot{\sigma}_n|_{\dot{\gamma}_s\to\infty} = \sigma_n\dot{\varepsilon}_n\left[(c_1 + c_2 + c_3)\nu_f + c_3\mu + c_4\sqrt{1 + \nu_f^2}\right] = 0 \tag{22}$$

where $\nu = \dot{\varepsilon}_n/\dot{\gamma}_s$. Combining Eqs. (19)–(22), and taking the fact that $\nu_f = 0$, the model coefficients $c_1$, $c_2$, $c_3$, $c_4$ can be solved:

$$\begin{cases} c_1 = G/(\sigma_{n0}I_{se0}), \quad c_2 = c_1\left[\frac{\sqrt{1+\nu_i^2}I_{e0}}{\mu\nu_i} - \left(1 + \frac{1}{\mu^2}\right)\right] \\ c_3 = c_1/\mu^2, \quad c_4 = -c_1/\mu \end{cases} \tag{23}$$

### Considerations of the Interface Roughness and Boundary Conditions

It is obvious that the roughness of the soil–structure interface can be a major factor that would affect the behaviors of the interface. The roughness of the soil–structure interface can be evaluated by (Kishida and Uesugi 1987)

$$R_n = \frac{R_{\max}(L = D_{50})}{D_{50}} \tag{24}$$

details can be found from Kishida and Uesugi (1987). However, the roughness of the interface is not considered as a parameter of the proposed model, instead, the critical friction angle ($\phi_c$) is used to represent the roughness of the interface which is more natural and it is similar to the friction angle in the Mohr–Coulomb model.

There are three typical boundary conditions in the laboratory interface experiments, according to the normal behavior of the soil–structure interface. (1) Constant normal load (CNL): the normal load remains a constant during the shearing, $\dot{\sigma}_n = 0$. (2) Constant volume (CV): the volume of the soil remains constant during the shearing, that is to say, no normal displacement is generated during the shearing, $\dot{\varepsilon}_n = 0$. (3) Constant normal stiffness (CNS): the relation between the incremental normal stress and incremental normal strain is represented by an elastic spring with the stiffness equal to $K$. It should be noted that all these three boundary conditions can be uninformed into one simple condition by the stiffness $K$:

$$\dot{\sigma}_n = -K\dot{\varepsilon}_n \tag{25}$$

Usually, the interface thickness is considered in the range of 5–15 times the mean particle diameter ($d_{50}$):

$$d_s = R_d d_{50} \quad (R_d \approx 5 \sim 15) \tag{26}$$

In the CNL condition, $\dot{\sigma}_n$ is fixed to zero, thus $K = 0$; in the CV condition, $\dot{\varepsilon}_n = 0$ is fixed to zero, thus $K = \infty$. Usually, the compressive normal stress is considered positive stress, thus there is a negative sign in the equation. Combining Eq. (25) and the first component of Eq. (13), we have

$$\begin{aligned} \dot{\sigma}_n &= I_{se}\left[(c_1 + c_2 + c_3)\sigma_n\dot{\varepsilon}_n + c_3\left(\tau_s\dot{\gamma}_s + \tau_t\dot{\gamma}_t\right) + c_4\sigma_n\|\dot{\boldsymbol{\varepsilon}}\|I_e\right] \\ &= -K\dot{\varepsilon}_n \end{aligned} \tag{27}$$

Eq. (27) is a function of $\dot{\varepsilon}_n$, it can be solved to

$$\dot{\varepsilon}_n = -\frac{d_1d_2 \pm d_3\sqrt{{d_1}^2 + d_4{d_2}^2 - d_4{d_3}^2}}{{d_2}^2 - {d_3}^2} \tag{28}$$

where

$$\begin{aligned} d_1 &= c_3(\tau_s\dot{\gamma}_s + \tau_t\dot{\gamma}_t)I_{se} \\ d_2 &= K + \sigma_n(c_1 + c_2 + c_3)I_{se} \\ d_3 &= c_4\sigma_n I_e I_{se} \\ d_4 &= (\dot{\gamma}_s)^2 + (\dot{\gamma}_t)^2 \end{aligned} \tag{29}$$

Now we can substitute Eq. (28) to Eq. (13) to calculate the incremental stresses.

### Summary of Model Parameters

The model parameters can be categorized into three groups: (1) basic parameters; (2) critical state parameters; (3) breakage parameters. All the model parameters proposed in this study are listed in Table 1.

### *Procedures of the Optimization-Based Uncertainty Quantification Framework*

Based on the preceding introduced uncertainty quantification framework and the enhanced hypoplastic interface model, the procedures of the optimization-based uncertainty quantification framework are summarized in Fig. 3. In this paper, the covariance matrix adaption evolution strategy (CMA-ES) algorithm is used to calibrate the model parameters. The CMA-ES is a randomized method of continuous optimization for nonlinear, nonconvex functions (Hansen and Ostermeier 1996; Hansen 2016). The CMA-ES algorithm has been implemented in various programming languages, such as C, C++, Fortran, Java, Matlab, R, and Scilab; this paper uses the Python implementation of the CMA-ES algorithm (Hansen 2023) to do the calibration.

## Results and Discussion

In this section, the Fontainebleau sand–steel interface experimental tests conducted by Pra-Ai (2013) will be evaluated. The properties of the sand used in the interface tests are listed in Table 2. The experimental tests are conducted with various normal stresses and void ratios, representing the soil is sheared under different stress states and density states.

### *Calibration of Fontainebleau Sand–Steel Interface Experiments*

The interaction of parameter uncertainty can often be studied by the MCS based on the analytical model where the parameters are sampled according to their statistical distributions. The results of the MCS are then used to describe the statistical properties of the model output (i.e., the factor of safety) which is the key to the reliability-based design (RBD) for the engineering applications. However, the statistical distributions of the model parameters are usually unknown since most parameters cannot be measured directly. In the following, the calibration of the parameter uncertainty is conducted based on the following assumptions.

1. The experiments are conducted with care, thus the measurement errors are negligible.
2. The analytical model can fully describe the behavior of the soil, thus the model bias is negligible.
3. The model parameters (model inputs) and predictions (model outputs) are assumed to be independently distributed with normal distributions for simplicity.

Based on the preceding assumptions, the Fontainebleau sand–steel interface experiments are calibrated using the previously introduced optimization-based calibration framework. Fig. 4 shows four typical examples of the uncertainty calibration results: (a) well-calibrated case with most observed data points within the 95% interval of the predictions and few outliers (CNS, dense sand, $K = 1{,}000$ kN/m, $\sigma_{n0} = 100$ kPa, normal stress curve); (b) underconfident case with a too wide 95% interval of the predictions (CNS, loose sand, $K = 1{,}000$ kN/m, $\sigma_{n0} = 100$ kPa, normal stress curve); (c) biased case with the average of the predictions biased from the observed data points (CNS, loose sand, $K = 1{,}000$ kN/m, $\sigma_{n0} = 100$ kPa, normal displacement curve); (d) overconfident case with a too narrow 95% interval of the predictions (CNS, Loose sand, $K = 5{,}000$ kN/m, $\sigma_{n0} = 310$ kPa, normal displacement curve). The reason for the failed calibrations may be due to (1) the measurement errors are ignored especially for measurements with small values such as the normal displacement in Fig. 4(d) which may cause predictions of other variables to be underconfident such as the shear stress in Fig. 4(b); (2) the model bias is not negligible, resulting in the bias of the average of the predictions, such as the normal displacement in Fig. 4(c); (3) the model parameters are not independent or normally distributed; and so forth.

Table 3 shows the calibrated distribution parameters based on the constant normal load experiment conducted on loose sand with the initial normal stress of 60 kPa and parameters with small uncertainties are ignored. Figs. 5–7 show the calibration results of the Fontainebleau sand–steel interface experiments. In these figures, each column represents the predictions and/or observations in measurements, quantiles, and histograms for shear stress, normal displacement, and normal stress (for constant normal stiffness experiments). The figures show that the uncertainties are well calibrated for most experiments. In the measurements–predictions figures, the predicted 95% confidence intervals cover most of the measured data points and there are a few outliers. In the probability histogram figures, the results show that the probability density of the normalized observations fit well with the density of the ideal normal distribution, proving that the assumption of the normal distribution for the system responses is reasonable. Furthermore, figures of the predictions and observations in quantiles can be used to validate the normality of the observations based on the KS test (Kolmogorov 1933; Smirnoff 1939). Since the quantile function is the inverse of the CDF, the distance between the observed and predicted CDFs equals the distance between the observed and

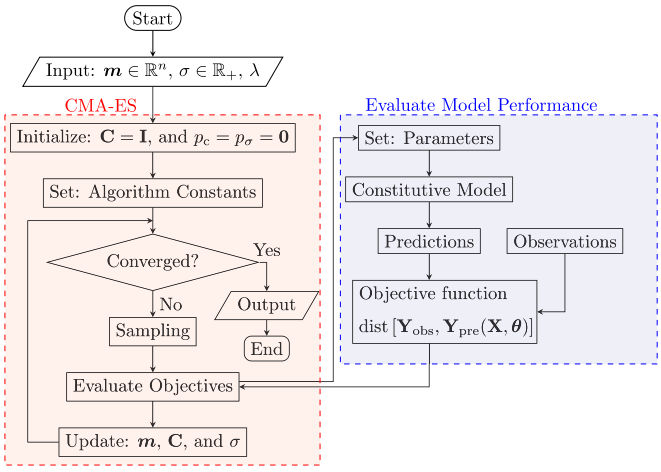


**Fig. 3.** Flowchart of the calibration of model parameters.

**Table 2.** Properties of sand used in the interface experiments

| BC | $D_{50}$ (mm) | $e_{max}$ | $e_{min}$ | $e$ | $K$ (kN/mm) | $\sigma_{n0}$ (kPa) |
|---|---|---|---|---|---|---|
| CNL | 0.23 | 0.866 | 0.545 | 0.76/0.57 | 0 | 60/120/310 |
| CNS | 0.23 | 0.866 | 0.545 | 0.76/0.57 | 1,000/2,000/5,000 | 100/310 |

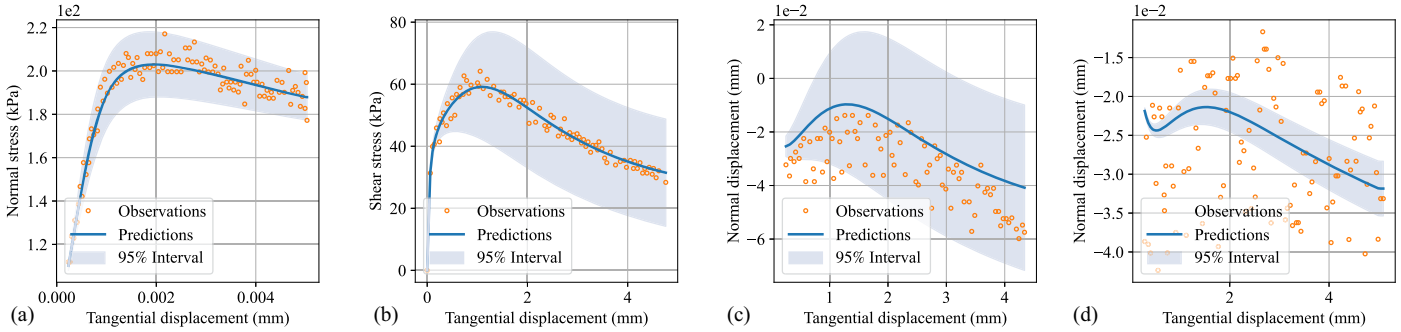


**Fig. 4.** Typical uncertainty calibration results: (a) well-calibrated case; (b) underconfident case; (c) biased case; and (d) overconfident case.

**Table 3.** Calibrated distribution parameters

| Parameter | $R_d$ | $\phi$ | $e_{refu}$ | $b$ | $\rho$ | $n_w$ | $\lambda$ | $\xi$ | $e_{ref0}$ | $n_p$ | $n_d$ | $G_0$ | $\nu_i$ |
|---|---|---|---|---|---|---|---|---|---|---|---|---|---|
| mean | 11.47 | 29.15 | 0.69 | 13913.33 | 11.29 | 1.90 | 0.06 | 0.79 | 0.77 | 0.00 | 1.51 | 542.54 | 1.00 |
| std | 0.35 | 1.60 | — | 7.71 | 0.53 | 0.01 | — | — | — | — | — | 2.27 | — |

predicted quantiles. Since the KS statistic measures the maximal distance between two CDFs, the KS statistic can be directly calculated as the maximal distance between the observed and predicted quantiles. Thus, assuming the confidence level to be 95%, the critical value of the KS statistic can be calculated and the corresponding intervals are plotted in the figures of the predictions and observations in quantiles. Experiments with observations–predictions curves in quantiles located within the confidence interval can be regarded to follow the normal distribution. In Figs. 5–7, it can be seen that the observations–predictions curves in quantiles of most experiments are within the confidence intervals (30 out of 42), proving that the framework is able to provide a reasonable estimation of the experimental uncertainties. The area between the observations–predictions curves and the ideal line $y = x$ can also be used to quantify whether the experiments are well calibrated. Table 4 shows the miscalibration area for different experiments. It can be seen that most of the experiments are well calibrated with a miscalibration area of less than 0.1.

Fig. 5 shows the calibration results for the constant normal load experiments. It can be seen that generally, the experimental uncertainties can be well predicted by introducing uncertainties in the model parameters. For normal displacement, the framework seems to predict the experiments well under different stress levels (60, 120, and 310 kPa) and densities (dense sand and loose sand)

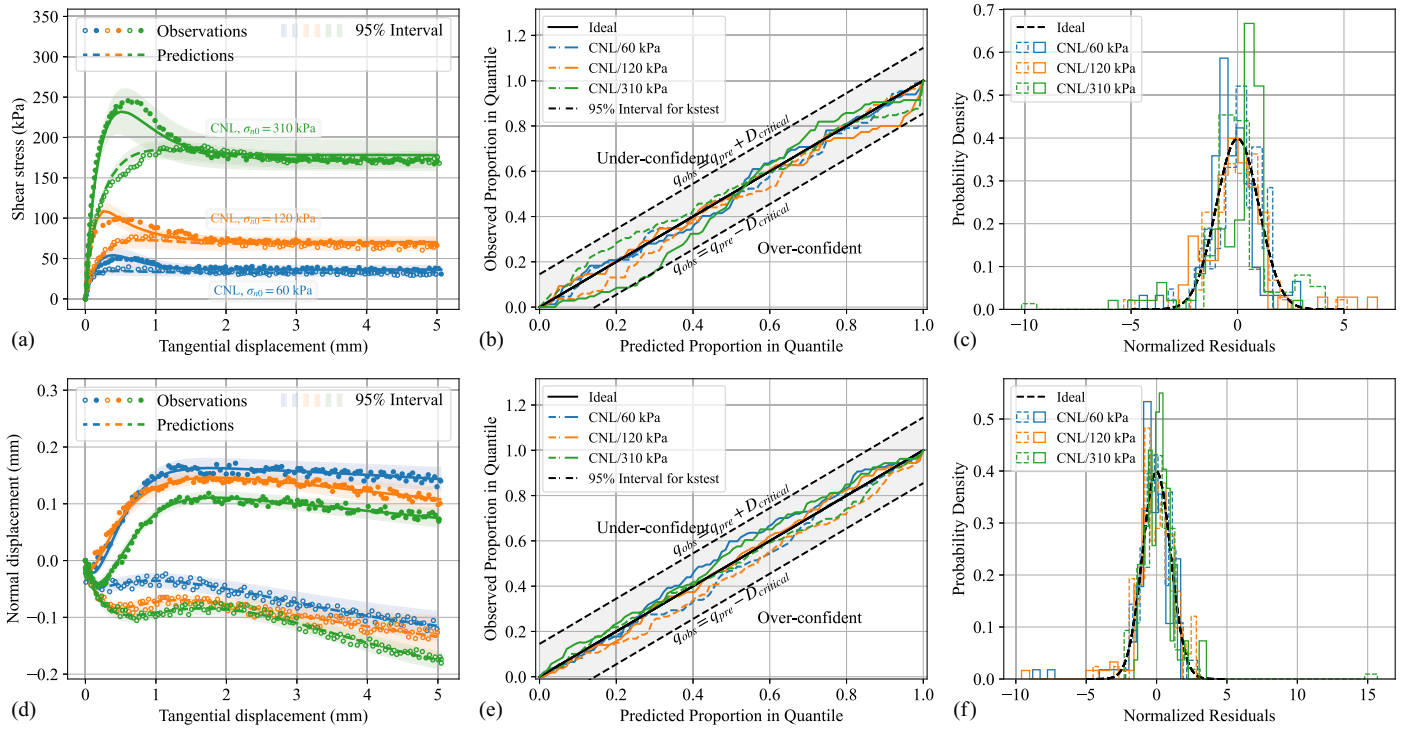


**Fig. 5.** Comparison between predictions and observations for constant normal load experiments: (a) shear stress in real measurements; (b) shear stress in quantiles; (c) shear stress in histograms; (d) normal displacement in real measurements; (e) normal displacement in quantiles; and (f) normal displacement in histograms.

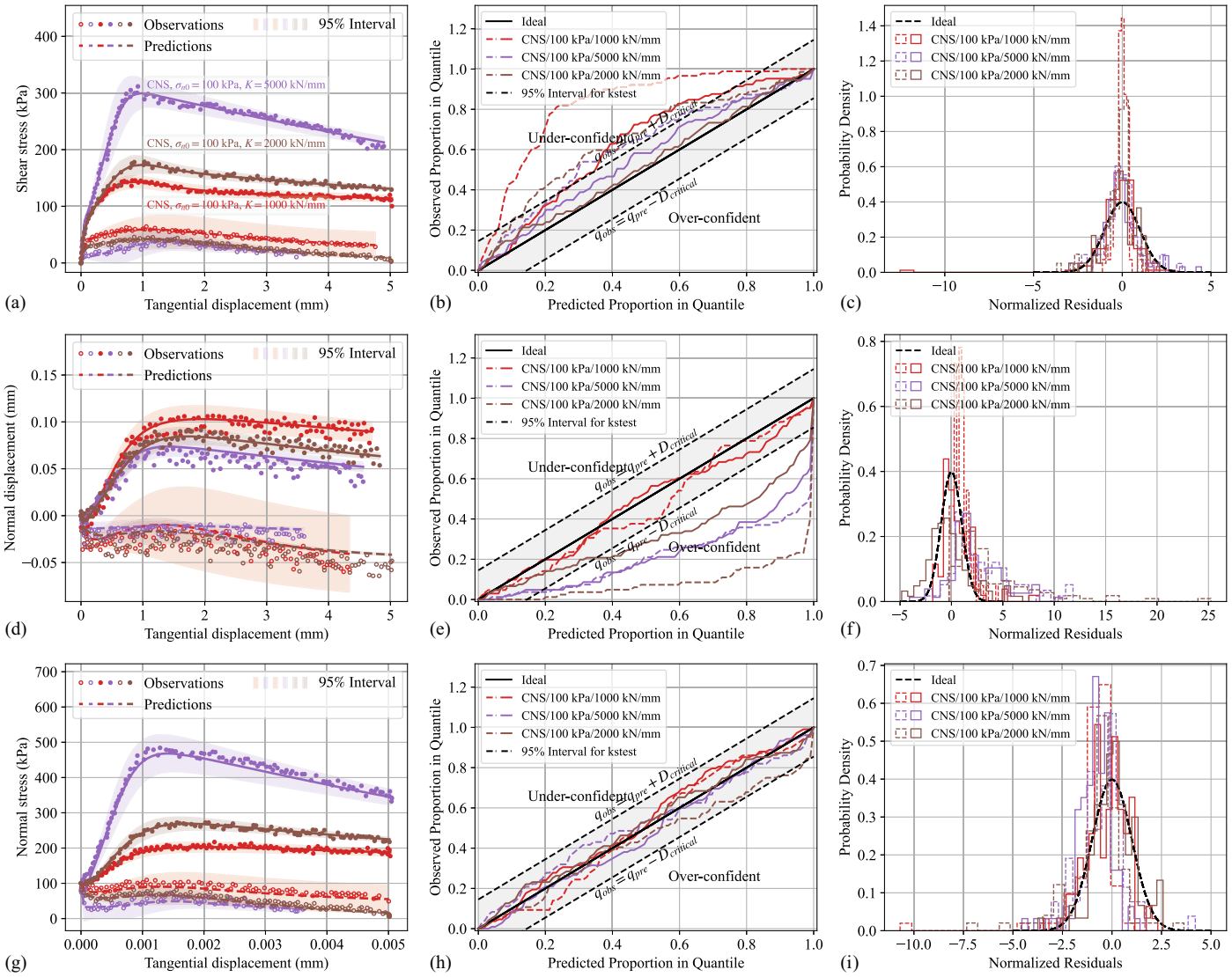


**Fig. 6.** Comparison between predictions and observations for constant normal stiffness experiments with initial normal stress of 100 kPa: (a) shear stress in real measurements; (b) shear stress in quantiles; (c) shear stress in histograms; (d) normal displacement in real measurements; (e) normal displacement in quantiles; (f) normal displacement in histograms; (g) normal stress in real measurements; (h) normal stress in quantiles; and (i) normal stress in histograms.

with the maximal miscalibration area of 0.067 [area between the predicted-observed quantile curve and the ideal curve $y = x$ in Fig. 5(e)]. Figures of predictions and observations in quantiles [Fig. 5(e)] and histograms [Fig. 5(f)] show that the observations fit well with the normal distribution and thus the preceding third assumption is proved to be reasonable. For shear stress, although the comparison between predictions and observations in quantiles (with the maximal miscalibration area of 0.069) and histograms show that the framework seems to be able to predict the experimental uncertainties, the predictions compared with the measurements seem to be underconfident (the confidence intervals are too wide) for experiments under a high-stress level (310 kPa), especially for experiments conducted on dense sand. However, the calibration metric used in this study seems unable to capture such mispredictions. This can be explained by the fact that the predictions are biased, and thus the second assumption cannot be ignored. The predictions are biased in different directions at different shearing stages (i.e., the shear stress is underestimated in the softening stage whereas it is overestimated in the hardening stage). However, due to the fact that the observed data points are limited, the observations are first normalized to follow the standard normal distributions, and then the observations in the whole shearing process are used to compare with the predictions, resulting in the ignorance of the stage information. Although the shortcoming can be reduced by conducting hundreds of parallel experiments and comparing the observations and predictions at every stage in the shearing process, it can be rather time-consuming and the model bias still cannot be ignored. Therefore, it can be concluded that the key to the framework is that the analytical model is the key to the success of the uncertainty calibration. The analytical model must be able to predict the experiments with satisfaction.

Figs. 6 and 7 show the calibration results for the constant normal stiffness experiments with the initial normal stress of 100 and 310 kPa. The calibration results of the constant normal stiffness experiments are clearly not as good as the calibration results of the constant normal load experiments due to the fact that additional normal stress is required to be fitted in the calibration. As shown in Figs. 6(b, e and h) and 7(b, e and h), it is interesting that for all constant normal stiffness experiments, the predictions for normal stress are usually well calibrated, whereas the predictions for shear stress are

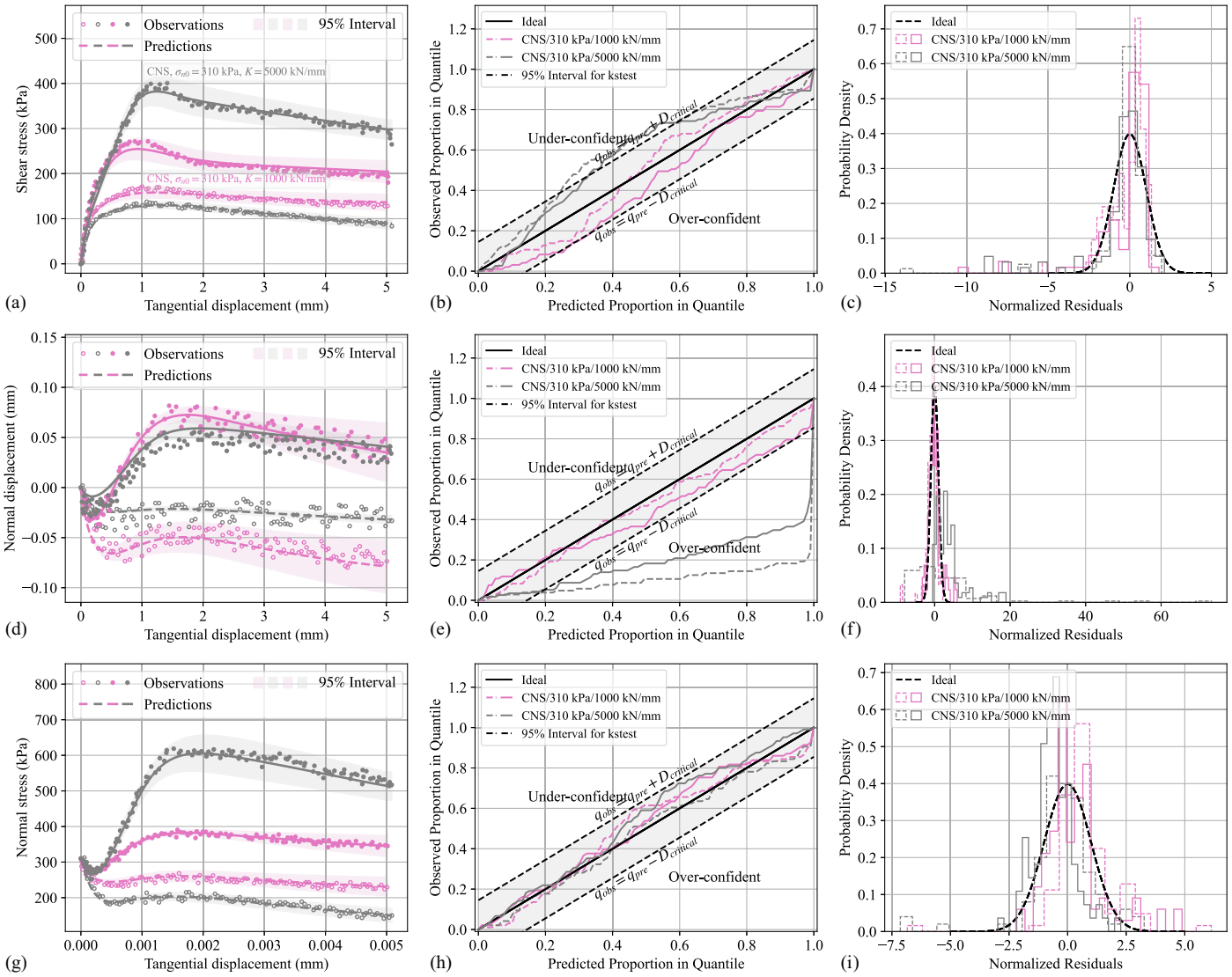


**Fig. 7.** Comparison between predictions and observations for constant normal stiffness experiments with initial normal stress of 310 kPa: (a) shear stress in real measurements; (b) shear stress in quantiles; (c) shear stress in histograms; (d) normal displacement in real measurements; (e) normal displacement in quantiles; (f) normal displacement in histograms; (g) normal stress in real measurements; (h) normal stress in quantiles; and (i) normal stress in histograms.

**Table 4.** Miscalibration area of the experiments

| BC | Initial normal stress | Stiffness | Density | Shear stress | Normal displacement | Normal stress |
|---|---|---|---|---|---|---|
| CNL | 60 | 0 | Loose | 0.02 | 0.04 | |
| | | | Dense | 0.03 | 0.04 | |
| | 120 | | Loose | 0.03 | 0.06 | |
| | | | Dense | 0.04 | 0.04 | |
| | 310 | | Loose | 0.06 | 0.02 | |
| | | | Dense | 0.07 | 0.04 | |
| CNS | 100 | 1,000 | Loose | 0.37 | 0.05 | 0.09 |
| | | | Dense | 0.14 | 0.05 | 0.04 |
| | | 2,000 | Loose | 0.19 | 0.43 | 0.06 |
| | | | Dense | 0.02 | 0.22 | 0.03 |
| | | 5,000 | Loose | 0.07 | 0.35 | 0.06 |
| | | | Dense | 0.06 | 0.29 | 0.03 |
| | 310 | 1,000 | Loose | 0.05 | 0.04 | 0.05 |
| | | | Dense | 0.09 | 0.08 | 0.05 |
| | | 5,000 | Loose | 0.11 | 0.44 | 0.04 |
| | | | Dense | 0.10 | 0.34 | 0.05 |

usually underconfident and the predictions for normal displacement are usually overconfident. Moreover, the fitting error decreases as the interface stiffness increases for shear stress, whereas it increases for the normal displacement. At the same time, it is different from the constant normal load experiments that the experiments conducted with loose sand are usually more difficult to be fitted in the calibration. It can be seen that for experiments with high interface stiffness and loose sand, the shear stress amplitudes are much smaller than in other experiments, whereas for experiments with low interface stiffness and loose sand, the normal displacement amplitudes are much smaller than in other experiments. The normal stress remains a rather high value for all experiments since it has an initial value. For these experiments with small amplitudes, the experimental uncertainties cannot be well calibrated using the proposed framework due to the fact that the experimental uncertainties are not only caused by the model parameters but also caused by other sources such as measurement errors that cannot be ignored.

In brief, the uncertainty calibration framework is able to identify the experimental uncertainties by considering the model parameters as the only uncertainty source. However, it has the following limitations corresponding to the assumptions.

1. The analytical model must be able to describe system responses accurately and thus the model bias can be ignored. Biased predictions cause the calibration metric to be unable to capture the stage-dependent information.
2. The measurement errors can be ignored. Experiments with higher amplitude variables are preferred since the relative measurement errors are smaller for higher amplitude variables.
3. The model parameters and system responses are assumed to be normally distributed. However, this assumption is not necessary and other distributions for the model parameters can be easily incorporated into the framework. For simple systems (i.e., linear systems), the distribution of the system responses can be exactly determined. For more complex systems, the distribution of the system responses cannot be exactly determined and it must be assumed. The correlations between model parameters are ignored to avoid numerous computational overhead.

### Discussion on Selection of Experiments for Calibration of Model Parameters

In engineering practice, one always wishes to conduct the fewest number of experiments to obtain the best performance. Generally speaking, at least three experiments are required to calibrate the model parameters. However, in the domain of soil–structure interface, more experiments are likely to be conducted to satisfy various loading and boundary conditions. The experiments under CNL are the simplest and are most widely studied in research. Considering the simplicity, the CNL tests be can very useful to calibrate the model parameters. However, to apply the model to CV (the normal displacement is fixed) tests and CNS (the normal stress–strain behavior is represented by an elastic spring, which is the intermediate state between CNL and CV) tests, one must conduct CNS or CV experiments to improve the applicability.

Theoretically, the model can be used in any stress levels and any boundary conditions; however, the calibration of model parameters might be tricky, and numerous experiments need to be conducted. Previous studies showed that the calibration performance with different stress levels and loading paths are different (Yin et al. 2017). In other words, the contributions of different experiments in improving the calibration performance are different. Then, in practice, those experiments with high contributions may be chosen for calibration, and there is no need to conduct those experiments with low contributions to the calibration, which will significantly reduce the number of experiments needed for calibration.

To figure out the contributions of different experiments in improving the calibration performance, so that it is possible to conduct a specific set of experiments to obtain the best performance with the fewest number of experiments, we choose some experiments in Table 2 for calibration, and the calibrated model parameters will be passed to other experiments for validation. Based on those sets of experiments for calibration with high validation performance, we could obtain information that what kinds or what combinations of experiments should be chosen for calibration of the hypoplastic model.

The number of experiments used for calibration remains an issue. Usually, at least three experiments must be conducted, and we do not wish to conduct more than five experiments. Thus, three to five experiments are chosen for calibration and the remaining 11–13 experiments will be used for validation. Based on some basic understanding of the selection strategy, selection sets of experiments for calibration are shown in Table 5.

The validation performance when different numbers of experiments are chosen for calibration are compared in Fig. 8. It can be concluded that increasing the number of experiments for model calibration will improve the performance of the validation, which is consistent with common knowledge. When five experiments are used for model calibration, the validation error is less than 20% over 60% of all the experiments groups, which is able to meet engineering requirements.

Table 6 shows the best sets of experiments when a different number of experiments is chosen. From Fig. 8, generally, we concluded that the validation performance is improved when more experiments are chosen for calibration. However, in Table 6, when we

**Table 5.** Groups of experiments for calibration

| Group | No. | BC | $K$ (kN/mm) | $\sigma_{n0}$ (kPa) | $e$ |
|---|---|---|---|---|---|
| 3 Experiments | 1 | CNL | 0 | 60/120/310 | 0.57/0.76 |
| | 2 | | | | |
| | 3 | CNS | 1,000/2,000/5,000 | 100/310 | 0.57/0.76 |
| 4 Experiments | 1 | CNL | 0 | 60/120/310 | 0.57/0.76 |
| | 2 | | | | |
| | 3 | CNS | 1,000/2,000/5,000 | 100 | 0.57/0.76 |
| | 4 | | 1,000/5,000 | 310 | |
| 5 Experiments | 1 | CNL | 0 | 60 | 0.57/0.76 |
| | 2 | | | 120 | |
| | 3 | | | 310 | |
| | 4 | CNS | 1,000/2,000/5,000 | 100 | 0.57/0.76 |
| | 5 | | 1,000/5,000 | 310 | |

Note: If a cell is empty, it adopts the same value as the upper cell.

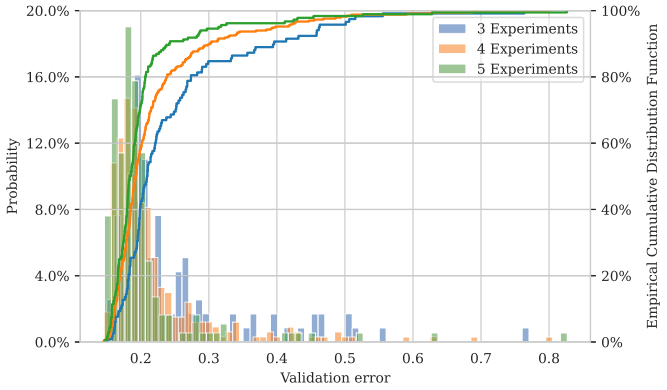


**Fig. 8.** Comparison of validation performance with a different number of experiments selected for calibration.

focus on the "best" sets of experiments, things might be a little different; the improvement of validation performance is not significant when more experiments are chosen for calibration. That is to say, the selection of experiments cares more about the types of experiments rather than the number of experiments. Even with a limited number of experiments, an acceptable performance can be achieved. The problem is, how can we choose a good set of experiments for calibration to obtain the best performance? Generally speaking, the selection is highly related to the real boundary or loading conditions that the model will be applied to, thus the selection of experiments must be incorporated with these conditions. For example, in this study, we want to validate whether the model can be applied to both CNL and CNS conditions in different stress levels. The selection of experiments should be based on these two conditions, that is to say, considering the following two strategies.

1. The experiments should be conducted under both CNL and CNS conditions.
2. The experiments should be conducted under different stress levels.

In Table 5, rather than categorize the experiments group with all of the mathematical combinations, we considered the first strategy, so that both CNL and CNS experiments are included in the experiments group. In Table 6, it can be seen that the best sets of experiments are all experiments under different stress levels, which is consistent with the second strategy.

**Table 6.** Best sets of experiments with a different number of experiments selected for calibration

| Category | CNL Experiments | | | CNS Experiments | | Validation Error |
|---|---|---|---|---|---|---|
| All experiments | D/L-60/120/310 | | | D/L-100/310-1,000/2,000/5,000 | | 13.8% |
| 3 Experiments | D-60 | D-310 | | L-5,000-100 | | 15.1% |
| | D-60 | L-310 | | D-1,000-310 | | 15.8% |
| | D-120 | L-310 | | D-1,000-100 | | 15.8% |
| 4 Experiments | D-60 | D-120 | | L-5,000-100 | D-5,000-310 | 14.5% |
| | D-120 | D-310 | | L-5,000-100 | D-5,000-310 | 14.7% |
| | D-120 | D-310 | | L-5,000-100 | L-1,000-100 | 14.8% |
| 5 Experiments | D-60 | D-120 | D-310 | L-5,000-100 | D-5,000-310 | 14.7% |
| | D-60 | D-120 | D-310 | L-5,000-100 | L-1,000-310 | 15.0% |
| | D-60 | D-120 | L-310 | L-5,000-100 | D-5,000-310 | 15.1% |

Note: D/L, dense/loose sand; 60/100/120/310, the normal stress; 1,000/2,000/5,000, the normal stiffness.

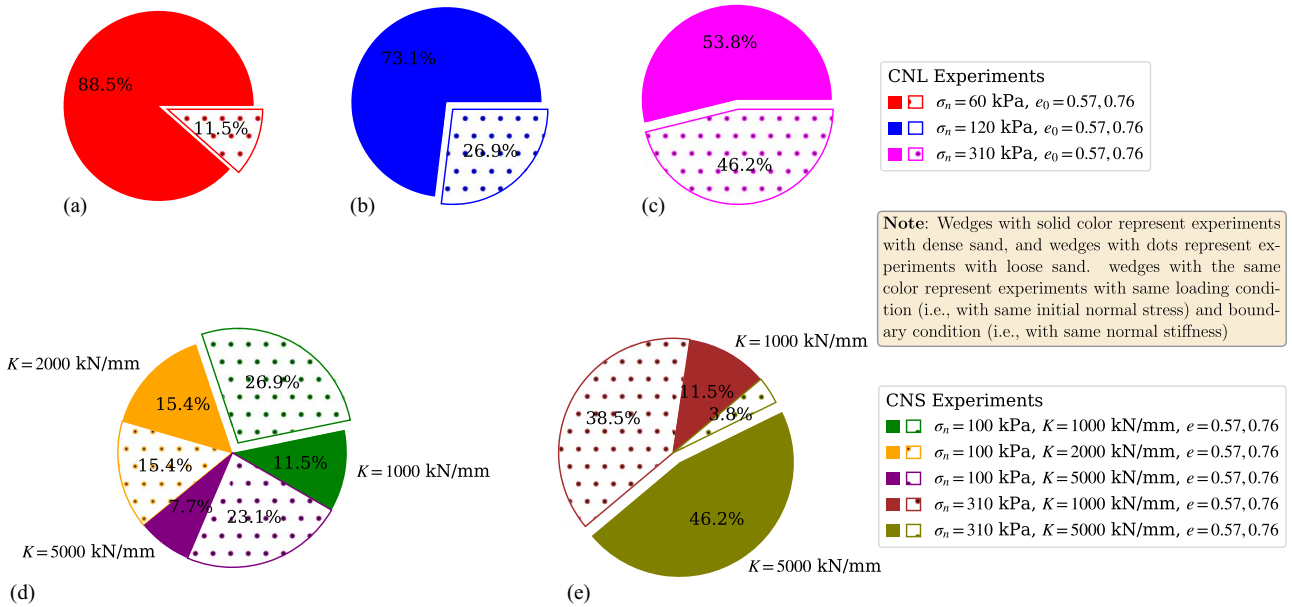


**Fig. 9.** Distribution of successfully calibrated sets of experiments: (a) CNL experiments with initial normal stress of 60 kPa; (b) CNL experiments with initial normal stress of 120 kPa; (c) CNL experiments with initial normal stress of 310 kPa; (d) CNS experiments with initial normal stress of 100 kPa; and (e) CNS experiments with initial normal stress of 310 kPa.



Int. J. Geomech., 2024, 24(6): 04024103

To investigate more about the selection of experiments for calibration, we have also done some research about those "successful experiment sets" (the validation error is less than 18%) when five experiments are chosen for calibration. The distribution of successfully calibrated sets of experiments is shown in Fig. 9. In the CNL condition in Figs. 9(a–c), among the successfully calibrated sets of experiments, over 70% experiments are experiments with dense sand, and there is a downward trend in the percentage of experiments with dense sand with the increase of the stress level. This is because in the dense sand, there will be a peak point in the shear strength line due to the dilatancy effect, which is controlled by the model parameter $n_p$. To simulate this effect, experiments with dense sand are required. With the increase of the stress level, the difference between dense sand and loose sand is getting larger, but to simulate the behavior of the loose sand, we would better choose more experiments with loose sand. However, in general, experiments should be focused on dense sand.

In the CNS condition, as shown in Figs. 9(c and d), it seems that the normal stiffness of the experiments have no significant effect on the calibration performance, when the initial normal stress is 100 kPa, among those successful sets of experiments, the proportions of experiments with different normal stiffness are approximately 40% ($K = 1{,}000$ kN/mm), 30% ($K = 2{,}000$ kN/mm), 30% ($K = 5{,}000$ kN/mm); for 310 kPa, they are 50% ($K = 1{,}000$ kN/mm), 50% ($K = 5{,}000$ kN/mm). Also, the difference between experiments with dense sand or loose sand is not that obvious. Under low-stress levels (i.e., 100 kPa), choosing experiments with loose sand seems like a good option, but under high-stress levels (310 kPa), the choice might depend on the normal stiffness. Choosing experiments with loose sand when the normal stiffness is low (i.e., 1,000 kN/mm) and choosing experiments with dense sand when the normal stiffness is high (i.e., 5,000 kN/mm) seems like a good option.

## Conclusions

To consider the uncertainties revealed in the experimental observations, a CMA-ES-based model calibration framework considering the uncertainties has been proposed by considering the model parameters and the numerical predictions as random variables. A two-dimensional MCS is required to obtain the optimal distribution parameters of the random variables. The outer loop of the MCS is used to sample the model parameters from their distributions, whereas the inner loop is used to quantify the difference between the predictions and the observations statistically. To improve the efficiency of the two-dimensional MCS, a simplified two-dimensional MCS with a fixed random structure in the inner loop is adopted, which also guarantees the calibration metric is stable so that the optimization algorithm can work properly. An enhanced hypoplastic soil–structure interface model has been proposed. By introducing the critical state concept, the particle breakage effect, and a nonlinear shear modulus to a simple hypoplastic model, the enhanced model is able to simulate the softening/hardening and breakage behaviors of the soil–structure interface. Combined with the CMA-ES optimization method, the model parameters considering uncertainties of the proposed model are identified based on the introduced calibration framework.

The results showed that the proposed uncertainty quantification framework is capable of calibrating the experimental uncertainties. For both constant normal load and constant normal stiffness experiments, the framework can capture the uncertainty revealed in the experiments with acceptable fitting errors. These results can be very useful in the reliability-based design in geotechnical engineering. However, because of the assumptions used in the framework, the framework must be used based on an analytical model that is able to accurately describe the system behaviors and the measurement error must be small enough to be negligible. The distributions of the model parameters and system responses are also required to be assumed to be used in the framework. Despite these limitations, the framework is able to capture the experimental uncertainties for most experiments considered in this paper. Furthermore, to figure out what kinds of experiments should be conducted when calibrating the model parameters when insufficient experiments can be conducted, some investigations have been done. The results showed that the selection of types of experiments can be critically important to the calibration of the model; CNL and CNS or CV experiments should be combined to improve the applicability of the model. Generally speaking, to apply the model to a wide range of boundary and loading conditions, experiments for calibration should be conducted under different stress levels and with different normal stiffness. Particularly, for CNL tests, we should focus on the experiments with dense sand when the hardening behavior will be revealed under low-stress levels, and under high-stress levels, experiments with loose sand can be conducted to further improve the performance. For CNS tests, under low-stress levels, choosing experiments with loose sand seems like a good option, but under high-stress levels, the choice might depend on the normal stiffness.

Due to the length limitation, the application of the approach in geotechnical practice, such as pile foundation and soil nailing, will be conducted as our future work.

## Data Availability Statement

All data of this study are available from the corresponding author upon reasonable request.

## Acknowledgments

This research was financially supported by the Research Grants Council (RGC) of Hong Kong Special Administrative Region Government (HKSARG) of China (Grant No. 15217220, N_PolyU534/20).

## References

Arnold, M., and I. Herle. 2006. "Hypoplastic description of the frictional behaviour of contacts." In *Numerical methods in geotechnical engineering*, 101–106. London: Taylor & Francis Group.

Brumund, W. F., and G. A. Leonards. 1973. "Experimental study of static and dynamic friction between sand and typical construction materials." *J. Test. Eval.* 1 (2): 162–165. https://doi.org/10.1520/JTE10893J.

Carbonari, S., M. Morici, F. Dezi, and G. Leoni. 2018. "A lumped parameter model for time-domain inertial soil–structure interaction analysis of structures on pile foundations." *Earthquake Eng. Struct. Dyn.* 47 (11): 2147–2171. https://doi.org/10.1002/eqe.v47.11.

Ching, J., and K.-K. Phoon. 2014. "Transformations and correlations among some clay parameters – the global database." *Can. Geotech. J.* 51 (6): 663–685. https://doi.org/10.1139/cgj-2013-0262.

Chung, Y., I. Char, H. Guo, J. Schneider, and W. Neiswanger. 2021. "Uncertainty toolbox: an open-source library for assessing, visualizing, and improving uncertainty quantification." Preprint, Accessed May 21, 2023. http://arxiv.org/abs/2109.10254.

DeJong, J. T., and Z. J. Westgate. 2009. "Role of initial state, material properties, and confinement condition on local and global soil–structure interface behavior." *J. Geotech. Geoenviron. Eng.* 135 (11): 1646–1660. https://doi.org/10.1061/(ASCE)1090-0241(2009)135:11(1646).

Desai, C. S., and Y. Z. Ma. 1992. "Modeling of joints and interfaces using the disturbed-state concept." *Int. J. Numer. Anal. Methods Geomech.* 16 (9): 623–653. https://doi.org/10.1002/nag.v16:9.
Desai, C. S., S. K. Pradhan, and D. Cohen. 2005. "Cyclic testing and constitutive modeling of saturated sand–concrete interfaces using the disturbed state concept." *Int. J. Geomech.* 5 (4): 286–294. https://doi.org/10.1061/(ASCE)1532-3641(2005)5:4(286).
D'Ignazio, M., K.-K. Phoon, S. A. Tan, and T. T. Länsivaara. 2016. "Correlations for undrained shear strength of finnish soft clays." *Can. Geotech. J.* 53 (10): 1628–1645. https://doi.org/10.1139/cgj-2016-0037.
Einav, I. 2007. "Breakage mechanics–Part I: Theory." *J. Mech. Phys. Solids* 55 (6): 1274–1297. https://doi.org/10.1016/j.jmps.2006.11.003.
Fakharian, K., and E. Evgin. 2000. "Elasto-plastic modelling of stress-path-dependent behaviour of interfaces." *Int. J. Numer. Anal. Methods Geomech.* 24 (2): 183–199. https://doi.org/10.1002/(ISSN)1096-9853.
Fender, J., F. Duddeck, and M. Zimmermann. 2014. "On the calibration of simplified vehicle crash models." *Struct. Multidiscip. Optim.* 49 (3): 455–469. https://doi.org/10.1007/s00158-013-0977-7.
Frost, J. D., J. T. DeJong, and M. Recalde. 2002. "Shear failure behavior of granular-continuum interfaces." *Eng. Fract. Mech.* 69 (17): 2029–2048. https://doi.org/10.1016/S0013-7944(02)00075-9.
Gneiting, T., F. Balabdaoui, and A. E. Raftery. 2007. "Probabilistic forecasts, calibration and sharpness." *J. R. Stat. Soc. B* 69 (2): 243–268. https://doi.org/10.1111/j.1467-9868.2007.00587.x.
Hansen, N. 2016. "The CMA evolution strategy: A tutorial." Preprint, Accessed May 15, 2023. http://arxiv.org/abs/1604.00772.
Hansen, N. 2023. "CMA-ES/pycma: r3.3.0." Accessed January 26, 2023. https://doi.org/10.5281/zenodo.7573532.
Hansen, N., and A. Ostermeier. 1996. "Adapting arbitrary normal mutation distributions in evolution strategies: The covariance matrix adaptation." In *Proc., IEEE Int. Conf. on Evolutionary Computation*, 312–317. Piscataway, NJ: IEEE Press.
Higdon, D., C. Nakhleh, J. Gattiker, and B. Williams. 2008. "A Bayesian calibration approach to the thermal problem." *Comput. Methods Appl. Mech. Eng.* 197 (29–32): 2431–2441. https://doi.org/10.1016/j.cma.2007.05.031.
Hofer, E., M. Kloos, B. Krzykacz-Hausmann, J. Peschke, and M. Woltereck. 2002. "An approximate epistemic uncertainty analysis approach in the presence of epistemic and aleatory uncertainties." *Reliab. Eng. Syst. Saf.* 77 (3): 229–238. https://doi.org/10.1016/S0951-8320(02)00056-X.
Hu, L. M., and J. L. Pu. 2003. "Application of damage model for soil–structure interface." *Comput. Geotech.* 30 (2): 165–183. https://doi.org/10.1016/S0266-352X(02)00059-9.
Hu, L. M., and J. L. Pu. 2004. "Testing and modeling of soil–structure interface." *J. Geotech. Geoenviron. Eng.* 130 (8): 851–860. https://doi.org/10.1061/(ASCE)1090-0241(2004)130:8(851).
Hu, W., Z. Yin, C. Dano, and P.-Y. Hicher. 2011. "A constitutive model for granular materials considering grain breakage." *Sci. China Technol. Sci.* 54 (8): 2188–2196. https://doi.org/10.1007/s11431-011-4491-0.
Jin, Y.-F., Z.-Y. Yin, Z.-X. Wu, and A. Daouadji. 2018a. "Numerical modeling of pile penetration in silica sands considering the effect of grain breakage." *Finite Elem. Anal. Des.* 144: 15–29. https://doi.org/10.1016/j.finel.2018.02.003.
Jin, Y.-F., Z.-Y. Yin, Z.-X. Wu, and W.-H. Zhou. 2018b. "Identifying parameters of easily crushable sand and application to offshore pile driving." *Ocean Eng.* 154: 416–429. https://doi.org/10.1016/j.oceaneng.2018.01.023.
Jung, B. C., H. Yoon, H. Oh, G. Lee, M. Yoo, B. D. Youn, and Y. C. Huh. 2016. "Hierarchical model calibration for designing piezoelectric energy harvester in the presence of variability in material properties and geometry." *Struct. Multidiscip. Optim.* 53 (1): 161–173. https://doi.org/10.1007/s00158-015-1310-4.
Kennedy, M. C., and A. O'Hagan. 2001. "Bayesian calibration of computer models." *J. R. Stat. Soc. B* 63 (3): 425–464. https://doi.org/10.1111/1467-9868.00294.
Kishida, H., and M. Uesugi. 1987. "Tests of the interface between sand and steel in the simple shear apparatus." *Géotechnique* 37 (1): 45–52.
Kleinberg, J., S. Mullainathan, and M. Raghavan. 2016. "Inherent trade-offs in the fair determination of risk scores." Preprint, Accessed May 21, 2023. http://arxiv.org/abs/1609.05807.
Kolmogorov, A. 1933. "Sulla determinazione empirica di una lgge di distribuzione." *Giorn. Inst. Ital. Attuari* 4: 83–91.
Kolymbas, D. 1991. "Computer-aided design of constitutive laws." *Int. J. Numer. Anal. Methods Geomech.* 15 (8): 593–604. https://doi.org/10.1002/nag.v15:8.
Koval, G., F. Chevoir, J. N. Roux, J. Sulem, and A. Corfdir. 2011. "Interface roughness effect on slow cyclic annular shear of granular materials." *Granular Matter* 13 (5): 525–540. https://doi.org/10.1007/s10035-011-0267-2.
Kullback, S., and R. A. Leibler. 1951. "On information and sufficiency." *Ann. Math. Stat.* 22 (1): 79–86. https://doi.org/10.1214/aoms/1177729694.
Lashkari, A. 2013. "Prediction of the shaft resistance of nondisplacement piles in sand." *Int. J. Numer. Anal. Methods Geomech.* 37 (8): 904–931. https://doi.org/10.1002/nag.v37.8.
Li, X.-S., and Y. Wang. 1998. "Linear representation of steady-state line for sand." *J. Geotech. Geoenviron. Eng.* 124 (12): 1215–1217. https://doi.org/10.1061/(ASCE)1090-0241(1998)124:12(1215).
Liu, F., M. Bayarri, J. Berger, R. Paulo, and J. Sacks. 2008. "A bayesian analysis of the thermal challenge problem." *Comput. Methods Appl. Mech. Eng.* 197 (29–32): 2457–2466. https://doi.org/10.1016/j.cma.2007.05.032.
Liu, Y.-J., G. Li, Z.-Y. Yin, C. Dano, P.-Y. Hicher, X.-H. Xia, and J.-H. Wang. 2014. "Influence of grading on the undrained behavior of granular materials." *C.R. Mec.* 342 (2): 85–95. https://doi.org/10.1016/j.crme.2013.11.001.
Mašín, D. 2015. "The influence of experimental and sampling uncertainties on the probability of unsatisfactory performance in geotechnical applications." *Géotechnique* 65 (11): 897–910.
Mortara, G. 2001. "An elastoplastic model for sand-structure interface behaviour under monotonic and cyclic loading." Ph.D. thesis, Dept. of Structural, Geotechnical and Building Engineering, Politecnico di Torino.
Muir Wood, D., and K. Maeda. 2008. "Changing grading of soil: Effect on critical states." *Acta Geotechnica* 3 (1): 3–14. https://doi.org/10.1007/s11440-007-0041-0.
Papaioannou, I., and D. Straub. 2017. "Learning soil parameters and updating geotechnical reliability estimates under spatial variability–theory and application to shallow foundations." *Georisk* 11 (1): 116–128.
Park, C., J.-H. Choi, and R. T. Haftka. 2016. "Teaching a verification and validation course using simulations and experiments with paper helicopters." *J. Verif. Validation Uncertainty Quantif.* 1 (3).
Phoon, K.-K. 2020. "The story of statistics in geotechnical engineering." *Georisk: Assess. Manage. Risk Eng. Syst.* 14 (1): 3–25.
Phoon, K.-K., and F. H. Kulhawy. 1999. "Characterization of geotechnical variability." *Canadian Geotechnical Journal* 36 (4): 612–624. https://doi.org/10.1139/t99-038.
Pra-Ai, S. 2013. "Behaviour of soil–structure interfaces subjected to large number of cycles. Application to piles." Ph.D. thesis, Doctoral School Engineering – Materials, Mechanics, Environment, Energy, Processes, Production (I-MEP2) Univ. de Grenoble.
Psarropoulos, P. N., Y. Tsompanakis, and M. Katsirakis. 2022. "Dynamic soil–structure interaction between retaining walls, retaining soil and retained structures." *Bull. Earthquake Eng.* 20 (7): 3593–3617. https://doi.org/10.1007/s10518-021-01288-6.
Richart, F. E., J. R. Hall, and R. D. Woods. 1970. *Vibrations of soils and foundations*. Upper Saddle River, NJ: Prentice Hall.
Roscoe, K. H., A. Schofield, and A. P. Wroth. 1958. "On the yielding of soils." *Geotechnique* 8 (1): 22–53. https://doi.org/10.1680/geot.1958.8.1.22.
Sayed, M. A., O.-S. Kwon, D. Park, and Q. Van Nguyen. 2019. "Multi-platform soil–structure interaction simulation of Daikai subway tunnel during the 1995 Kobe earthquake." *Soil Dyn. Earthquake Eng.* 125: 105643. https://doi.org/10.1016/j.soildyn.2019.04.017.
Seo, H. J., and L. Pelecanos. 2018. "Finite element analysis of soil–structure interaction in soil anchor pull-out tests." In *Numerical*

*methods in geotechnical engineering IX*, 1439–1444. Boca Raton, FL: CRC Press.
Singh, V. P., and G. SivakumarBabu. 2010. "2d numerical simulations of soil nail walls." *Geotech. Geol. Eng.* 28 (4): 299–309. https://doi.org/10.1007/s10706-009-9292-x.
Skau, K. S., H. P. Jostad, G. Eiksund, and H. Sturm. 2019. "Modelling of soil–structure-interaction for flexible caissons for offshore wind turbines." *Ocean Engng* 171: 273–285. https://doi.org/10.1016/j.oceaneng.2018.10.035.
Smirnoff, N. 1939. "On the estimation of the discrepancy between empirical curves of distribution for two independent samples." *Bull. Math. Univ. Moscou* 2 (2): 16.
Stutz, H., and D. Masin. 2017. "Hypoplastic interface models for fine-grained soils." *Int. J. Numer. Anal. Methods Geomech.* 41 (2): 284–303. https://doi.org/10.1002/nag.v41.2.
Stutz, H., D. Masin, and F. Wuttke. 2016. "Enhancement of a hypoplastic model for granular soil–structure interface behaviour." *Acta Geotech.* 11 (6): 1249–1261. https://doi.org/10.1007/s11440-016-0440-1.
Tang, W. H. 1984. "Principles of probabilistic characterization of soil properties." In *Geotechnical safety and reliability*, 39–39. Reston, VA: ASCE.
Uesugi, M., and H. Kishida. 1986. "Influential factors of friction between steel and dry sands." *Soils Found.* 26 (2): 33–46. https://doi.org/10.3208/sandf1972.26.2_33.
Wang, S., W. Wu, Z.-Y. Yin, C. Peng, and X. He. 2018. "Modelling the time-dependent behaviour of granular material with hypoplasticity." *Int. J. Numer. Anal. Methods Geomech.* 42 (12): 1331–1345. https://doi.org/10.1002/nag.v42.12.
Warner, J. E., W. Aquino, and M. D. Grigoriu. 2015. "Stochastic reduced order models for inverse problems under uncertainty." *Comput. Methods Appl. Mech. Eng.* 285: 488–514. https://doi.org/10.1016/j.cma.2014.11.021.
Wu, W., and E. Bauer. 1994. "A simple hypoplastic constitutive model for sand." *Int. J. Numer. Anal. Methods Geomech.* 18 (12): 833–862. https://doi.org/10.1002/nag.v18:12.
Wu, Z.-X., Z.-Y. Yin, Y.-F. Jin, and X.-Y. Geng. 2019. "A straightforward procedure of parameters determination for sand: A bridge from critical state based constitutive modelling to finite element analysis." *Eur. J. Environ. Civ. Eng.* 23 (12): 1444–1466. https://doi.org/10.1080/19648189.2017.1353442.
Yang, J., and Z.-Y. Yin. 2021a. "Soil-structure interface modeling with the nonlinear incremental approach." *Int. J. Numer. Anal. Methods Geomech.* 45 (10): 1381–1404. https://doi.org/10.1002/nag.v45.10.
Yang, J., and Z.-Y. Yin. 2021b. "Soil-structure interface modeling with the nonlinear incremental approach." *Int. J. Numer. Anal. Methods Geomech.* 45 (10): 1381–1404. https://doi.org/10.1002/nag.v45.10.
Yasufuku, N., and H. Ochiai. 2005. "Sand-steel interface friction related to soil crushability." In *Geotechnical special publication*, 627–641. Reston, VA: ASCE.
Yin, Z.-Y., C. S. Chang, and P.-Y. Hicher. 2010. "Micromechanical modelling for effect of inherent anisotropy on cyclic behaviour of sand." *Int. J. Solids Struct.* 47 (14–15): 1933–1951. https://doi.org/10.1016/j.ijsolstr.2010.03.028.
Yin, Z.-Y., Y.-F. Jin, S.-L. Shen, and H.-W. Huang. 2017. "An efficient optimization method for identifying parameters of soft structured clay by an enhanced genetic algorithm and elastic–viscoplastic model." *Acta Geotech.* 12 (4): 849–867. https://doi.org/10.1007/s11440-016-0486-0.
Yin, Z. Y., Z. X. Wu, and P. Y. Hicher. 2018. "Modeling monotonic and cyclic behavior of granular materials by exponential constitutive function." *J. Eng. Mech.* 144 (4): 04018014. https://doi.org/10.1061/(ASCE)EM.1943-7889.0001437.
Youn, B. D., B. C. Jung, Z. Xi, S. B. Kim, and W. Lee. 2011. "A hierarchical framework for statistical model calibration in engineering product development." *Comput. Methods Appl. Mech. Eng.* 200 (13–16): 1421–1431. https://doi.org/10.1016/j.cma.2010.12.012.
Zhan, Z., Y. Fu, R.-J. Yang, and Y. Peng. 2011. "An automatic model calibration method for occupant restraint systems." *Struct. Multidiscip. Optim.* 44 (6): 815–822. https://doi.org/10.1007/s00158-011-0671-6.
Zhang, L., L. M. Zhang, and W. Tang. 2009. "Uncertainties of field pullout resistance of soil nails." *J. Geotech. Geoenviron. Eng.* 135 (7): 966–972. https://doi.org/10.1061/(ASCE)GT.1943-5606.0000014.
Zhang, L., Y. Zheng, and J. Wang. 2003. "Errors in calculating hydrodynamic pressures for stability analysis of soil slopes subject to rainfall." In *Proc. 9th Int. Conf. on Applications of Statistics and Probability in Civil Engineering*., 1431–1438. Fairfax, VA: IOS Press.